The effect of different step-size on the visualization of crystallographic defects using SEM/EBSD technique

Yoshikazu HIGA*, Ken SHIMOJIMA and Takashi MAKISHI
Department of Mechanical Systems Engineering,
Okinawa National College of Technology, 905 Henoko,
Nago, Okinawa, Japan

ABSTRACT
Crystallographic grains and defects play an important role in many fundamental processes, such as grain growth and recrystallization, damage, and plastic deformation. Due to the importance of these processes, there is considerable interest in characterizing the crystallographic orientation and grain boundary distribution of crystalline materials. In this study, crystallographic defects such as dislocation arrays and grain boundaries and their orientations were investigated in a commercial polycrystalline copper sample using electron backscatter diffraction (EBSD) mapping combined with scanning electron microscopy (SEM). EBSD was used to determine the local orientations at individual points of a regular grid on a planar surface of a specimen. From the orientation differences between neighboring points, the lattice curvature and dislocation density tensor were derived, and the dislocation density distribution accompanying the crystallographic defects was significantly dependent on the SEM/EBSD step size associated with the spatial resolution.

Keywords: Crystallographic defects, Lattice curvature/dislocation density tensor, SEM/EBSD, Step size

1. INTRODUCTION

There have been many experimental observations and interesting reports in computational material science based on recent technological developments in micro- to nano-scale observations. Electron beam tomography has been used for in-situ three-dimensional observation of lattice defects in crystallographic metals associated with the elementary processes of plastic deformation [1, 2]. For the dislocation density tensor associated with the strain-gradient-dependent crystal plasticity theorem, a technique using white X-ray diffraction for estimating the geometrically necessary dislocation density were developed [3]. Calculations of the dislocation density distribution obeying the curvature tensor in the crystal lattice have been performed on the basis of SEM/EBSD and FIB/EBSD observations [4–6]. The EBSD scheme used in this study can estimate the curvature tensor using the spatial gradient associated with each observation point, the crystallographic orientation data, and its difference. Therefore, any estimation of the curvature tensor should be strongly dependent on the method used to calculate the spatial gradient and also on the number of observation points in its region. To our knowledge, the research in this viewpoint has been very little.

*Corresponding Author: E-mail: y.higa@okinawa-ct.ac.jp

This study, involving the visualization of lattice defects in crystalline metals using dislocation density tensor maps, explores the effect of number of observation points on the estimating the curvature and the dislocation density tensor.

2. BASIC RELATION BETWEEN CURVATURE AND DISLOCATION DENSITY TENSOR

The orientation of a crystalline lattice is described by the rotation required to reach this orientation from a chosen reference orientation [7]. This rotation is most frequently characterized by the Bunge rotation matrix **g** [8] based on the Euler angles (ϕ_1, Φ, ϕ_2), as shown in Eq. (1). When calculating the distortion of crystallographic structures, one can consider only the rotation component of the lattice strain, because the elastic component should be negligible. Therefore, using the rotation matrix shown in Eq. (1), one can obtain the following equation:

$$g_{ij} = \begin{bmatrix} \cos\phi_1 \cos\phi_2 - \sin\phi_1 \sin\phi_2 \cos\Phi & \sin\phi_1 \cos\phi_2 + \cos\phi_1 \sin\phi_2 \cos\phi & \sin\phi_2 \sin\Phi \\ -\cos\phi_1 \sin\phi_2 - \sin\phi_1 \sin\phi_2 \cos\Phi & -\sin\phi_1 \sin\phi_2 + \cos\phi_1 \cos\phi_2 \cos\Phi & \cos\phi_2 \sin\Phi \\ \sin\phi_1 \sin\Phi & -\cos\phi_1 \sin\Phi & \cos\Phi \end{bmatrix} \quad (1)$$

$$\omega_{ij} = g_{ij} - \delta_{ij} \quad (2)$$

where δ_{ij} represents the Kronecker delta.

Using Eq. (2), the lattice rotation vector θ can be determined as follows:

$$\theta_k = -\varepsilon_{kij}\omega_{ij}/2 \quad (3)$$

where ε_{ijk} is the Levi-Civita permutation symbol.

From the above, one can obtain the curvature tensor κ from the spatial gradient of the lattice rotation vector as follows:

$$\kappa_{ij} = \frac{\partial\theta_i}{\partial x_j} \approx 2\frac{\Delta q_i}{\Delta x_j} \quad (4)$$

where $\Delta\boldsymbol{q}$ and $\Delta\mathbf{x}$ indicate the difference in crystallographic orientation and the distance between two neighboring points, respectively. $\Delta\boldsymbol{q}$, the difference between one orientation (A) and another orientation (B) can be expressed by the quaternion product [6]:

$$\Delta\boldsymbol{q} = \boldsymbol{q}_B\boldsymbol{q}_A^{-1} = \begin{pmatrix} q_0^B q_0^B + \boldsymbol{q}^B \cdot \boldsymbol{q}^B \\ -q_0^B\boldsymbol{q}^A + \boldsymbol{q}^B q_0^A - \boldsymbol{q}^B \times \boldsymbol{q}^A \end{pmatrix} \quad (5)$$

where q_A^{-1} denotes the inverse quaternion corresponding to the value of the conjugate quaternion divided by its norm. Here, the quaternion consists of a scalar q_0 and a vector $\boldsymbol{q} = (q_1, q_2, q_3)$. One can also obtain the following equation using the Bunge rotation matrix $\boldsymbol{g}$ given by Eq. (1):

$$q_0 = \frac{1}{2}\sqrt{g_{ii}+1}, q_i = -\frac{1}{4q_0}\varepsilon_{ijk}g_{jk} \quad (6)$$

Therefore, one can obtain the curvature tensor using Eq. (4) along with the crystallographic orientation data. Then, the dislocation density tensor can be estimated as:

$$\alpha_{ij} = \kappa_{ji} - \delta_{ij}\kappa_{kk} \quad (7)$$

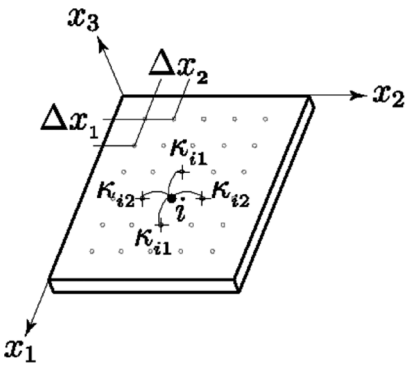

Figure 1: A sketch of the sample coordinate system used for EBSD. The curvature tensor with respect to point "*i*" is determined by the central difference at each of the cross arranged in a square lattice on the surface of the specimen

$$\left.\begin{array}{ccc} & \alpha_{12} = \kappa_{21} & \alpha_{13} = \kappa_{31} \\ \alpha_{21} = \kappa_{12} & & \alpha_{23} = \kappa_{32} \\ & & \alpha_{33} = -\kappa_{11} - \kappa_{22} \end{array}\right\} \tag{8}$$

The dislocation density tensor associated with the above curvature tensor calculation cannot estimate the spatial gradient in the thickness direction, because the crystallographic orientation data obtained from SEM/EBSD is surface data, as shown in Figure 1. Hence, there are six evaluable components of the curvature tensor (κ_{11}, κ_{21}, κ_{31}, κ_{12}, κ_{22} and κ_{32}) Consequently, there are five measurable components of the dislocation density tensor, (α_{12}, α_{13}, α_{21}, α_{23} and α_{33}) as shown in Eq. (8).

3. OBSERVATION SAMPLE AND ITS CONDITIONS

This study employed oxygen-free copper (C1011) to calculate defect information from the spatial gradient of the crystallographic orientation. The specimens were 10.0 mm in diameter and 2.2 mm thick.

To remove the damaged layer and coarsen the grains for easier observation, the specimen was annealed in a furnace. The inside of the furnace was kept under a high vacuum, and heated to 900ºC. This temperature was maintained for 24 hr, and then the sample was naturally cooled in the furnace. After annealing, electropolishing was performed under the conditions listed in Table 1, to obtain an acceptable surface quality. Using this sample, the crystallographic orientation data were determined using SEM/EBSD under the conditions shown in Table 2. In order to investigate the effect of the SEM/EBSD step size on the estimation of the spatial gradient, the crystallographic orientation was determined using "SQUARE GRID", which is similar to the finite difference method, for the same region. The step sizes were 1, 2, and 4 μm, and the sample region was 400 × 400 μm^2. Additional experimental conditions of the SEM/EBSD measurements are shown in Table 2.

The crystallographic orientation and the coordinates of each observation point were obtained using a postprocessor (OIM Analysis Ver. 4.6 ®TSL). Text-format data were also obtained for all of the observation points. Thus, calculations of Eqs. (4) and (7) could be performed. In this study, data with a CI (confidence index) value of less than 0.1 were discarded. Table 3 lists the number of data points with CI values above and below 0.1 for each step size examined.

Table 1: Electropolishing conditions

Solution	**H_3PO_4 : H_2O = 1 : 1**
Temperature	R.T.
Cathode	Copper
Voltage	2.0 V
Current	0.70 A
Time	120 sec

Table 2: Experimental conditions for SEM/EBSD

Acceleration voltage	**Vacc = 25 kV**
Working Distance	15.0 mm
Step Size, μm	1.0 2.0 4.0
Exposure area	400 × 400 μm^2
Exposure time	0.03 sec
Binning	4 × 4
Grid	SQUARE

Table 3: The number of data points

	Num. Points	
Step size, μm	**CI ≥ 0.1**	**CI < 0.1**
1.0	160358	443
2.0	40329	72
4.0	10186	15

4. EXPERIMENTAL RESULTS

4.1 CRYSTALLOGRAPHIC ORIENTATION OF THE SPECIMEN

The orientations were determined by SEM/EBSD at points on a regular "SQUARE GRID", with a mutual spacing of 1μm. Figures 2(a) and (b) show the obtained grain boundary map and inverse polar figure, respectively. The former shows the differences in crystallographic orientation between neighboring observation points. The green line indicates a low-angle boundary, with a 5–15 degree difference in crystallographic orientation. The blue line indicates a greater than 15 degree boundary, such as grain boundary. In this figure, a grain boundary clearly divides the left portion of the observation area from the right. Furthermore, the left and right regions had individual crystallographic orientations, as shown in Fig. 2(b).

4.2 LATTICE DEFECTS OBSERVATION USING A DISLOCATION DENSITY MAP

The obtainable components of the dislocation density tensor are illustrated in Fig. 3. To show the characteristic distribution of the dislocation density tensor, the range of the dislocation density tensors ranged from -1.0×10^6 to 1.0×10^6 m^{-1}. The higher-valued dislocation density tensors, α_{12}, α_{13} and α_{23}, were distributed in neighboring grain and Right Grain near the grain boundary. Furthermore, α_{21} and α_{33} were significantly distributed in Left Grain. The α_{33} component of the dislocation density tensor has a larger magnitude than the other components, because it contains the summations α_{11} and α_{22}, as shown in equation (8).

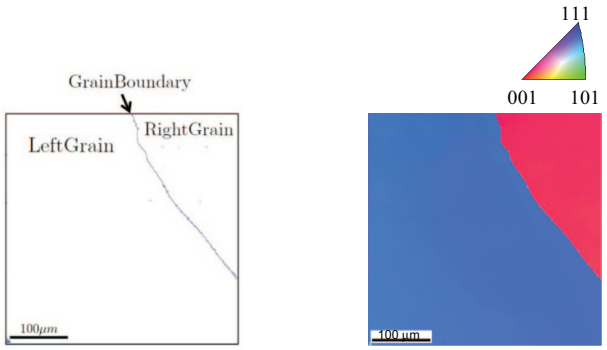

(a) Grain boundary map (b) Inverse pole figure map

Figure 2: Crystallographic orientation maps of the copper specimen

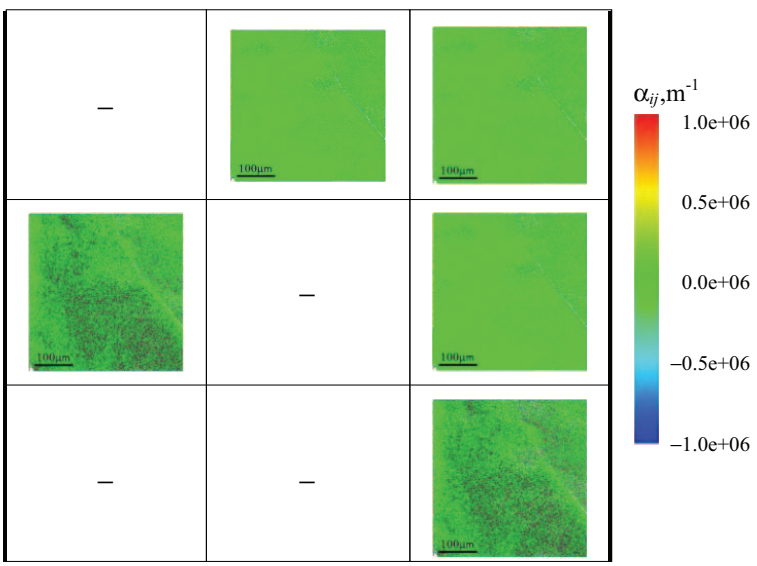

Figure 3: The five obtainable components of the dislocation density tensor, α_{ij}

Next, the average dislocation density ρ^*, also called the "apparent" dislocation density [5, 6], can be estimated by:

$$\rho^* = \frac{1}{|\mathbf{b}|}\left(|\alpha_{12}| + |\alpha_{13}| + |\alpha_{21}| + |\alpha_{23}| + |\alpha_{33}|\right) \tag{9}$$

where **b** is the Burger's vector associated with the copper lattice constant, a = 0.3615 nm [7]. Therefore, the magnitude of the Burger's vector |**b**| is 0.2556 nm.

Figure 4 shows a dislocation density map illustrating the "apparent" dislocation density. Comparing Figs. 4 and 2, the magnitude of the dislocation density at the grain boundary is remarkably larger than that in the grain interior. This is because of an increase in the quaternion $\Delta \boldsymbol{q}$ used to calculate the curvature tensor due to the magnitude of the

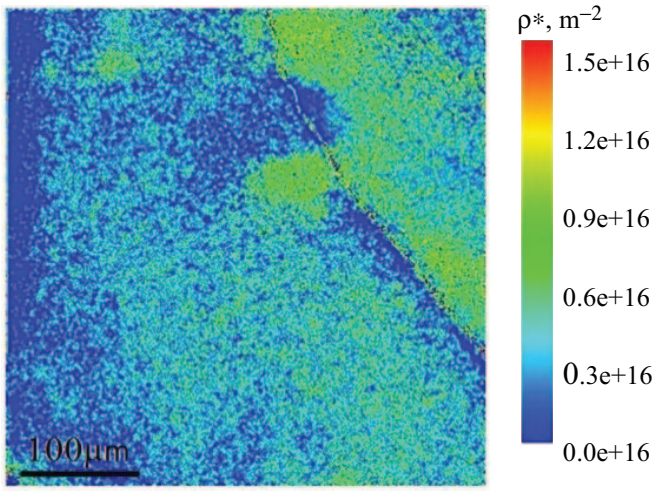

Figure 4: Dislocation density map

misorientation at near the grain boundary. Consequently, the value of the dislocation density related to the curvature tensor increases. In contrast, at Right Grain, a high dislocation density distribution was observed within the grain, but this cannot be confirmed from the inverse pole figure shown in Fig. 2. This suggests that the local defect distribution can be determined by calculating the curvature tensor from SEM/EBSD measurements.

4.3 STEP-SIZE DEPENDENCE OF DISLOCATION DENSITY CALCULATIONS

To clarify the effect of step size on the calculated dislocation density maps, we performed each step of 2 and 4 μm for getting the EBSD data at same square region, 400 × 400 μm^2. Figure 5 shows dislocation density maps for step sizes of 1, 2, and 4 μm. The dislocation densities ranged from 0 to 4.5 × 10^{15} m^{-2}. Regardless of the step size, we can see that there are the grain boundary divided by Left/Right Grain, the distribution and its localization of crystallographic defect. In contrast, the dislocation density decreased as the step size increased. In this study, we assumed the average dislocation density is estimated as dividing the sum of the dislocation density at observation point by its numbers. Figure 6 shows a double logarithmic graph relating the average dislocation density to the step sizes listed in Table 3. As a result, the

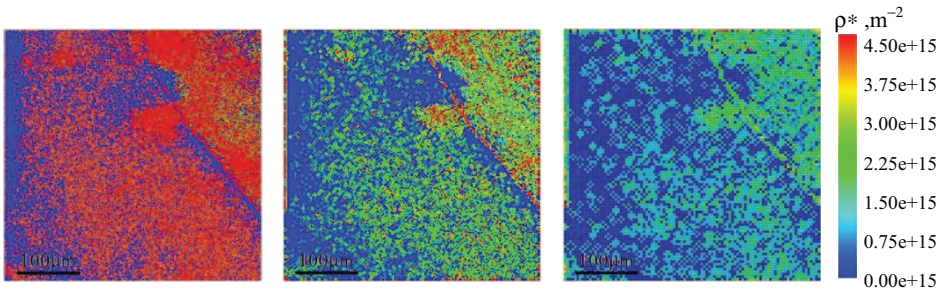

(a) 1.0 μm (b) 2.0 μm (c) 4.0 μm

Figure 5: Dislocation density maps for several SEM/EBSD step sizes

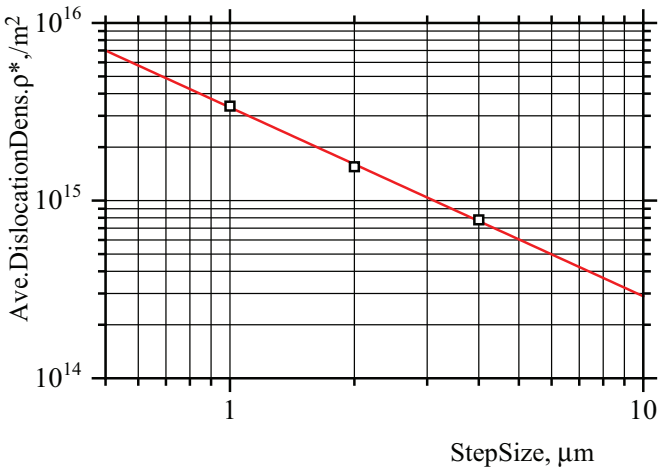

Figure 6: The log-log relationship between the average dislocation density and the SEM/EBSD step size

average dislocation density at any step size can be predicted. For example, the average dislocation density would be approximately 7.0×10^{15} m^{-2} for a 0.5 μm step size. Meanwhile, it is well known that the spatial resolution of EBSD is 10^2 to 10^3 times as large as the atomic order [7]. Therefore, the average dislocation density will be predictable if the crystallographic orientation data can be obtained using a high-resolution step size on the 10^{-1} order.

5. CONCLUSION

To visualize crystallographic defects using SEM/EBSD, the curvature and dislocation density tensor associated with spatial gradient were calculated. Dislocation density maps corresponding to the crystallographic defects were obtainable using EBSD. The following results were obtained in this study:

- ✓ One can visualize dislocation density maps related to crystalline defects. These dislocation density maps show not only the obvious grain boundaries, but also show the local distribution of crystalline defects in the individual grains.
- ✓ To clarify the step size dependence of this SEM/EBSD scheme, experiments were performed using different step sizes. The EBSD step size and the average dislocation density had an double logarithmic relationship. The dislocation density decreased as the step size increased, suggesting that the average dislocation density is predictable, if high-resolution crystallographic orientation data can be obtained, with a step size on the 10^{-1} order.

ACKNOWLEDGMENTS

The authors would like to express their sincere thanks to Mr. Takuya SUNAGAWA and Mr. Hiroto TERUYA for their tremendous effort in experimental study.

REFERENCES

[1] Barnard, J. S., Sharp, J., Tong, J. R. and Midgley, P. A. High-Resolution Three-Dimensional Imaging of Dislocation, *Science*, 2006, 313, 319.

[2] Hata, S., Kimura, K., Gao, H., Matsumura, S., Doi, M., Moritani, T., Barnard, J. S., Tong, J. R., Sharp, J. and Midgley, P. A. Electron Tomography Imaging and Analysis

of γ' and γ domains in Ni-based Superalloys, *Advanced Materials*, 2008, 20, 1905–1909.

[3] Barabash, R. I., Ice, G. E. and Pang, J. W. L. Gradients of geometrically necessary dislocations from white beam microdiffraction, *Materials Science and Engineering*, 2005, A400–401, 125–131.

[4] Field, D. P., Trivedi, P. B., Wright, S. I. and Kumar, M. Analysis of local orientation gradients in deformed single crystals, *Ultramicroscopy*, 2005, 103, 33–39.

[5] Pantleon, W. Resolving the geometrically necessary dislocation content by conventional electron backscattering diffraction, *Scripta Materialia*, 2008, 58, 994–997.

[6] He, W., Ma, W. and Pantleon, W. Microstructure of individual grains in cold-rolled aluminum from orientation inhomogeneities resolved by electron backscattering diffraction, *Materials Science and Engineering*, 2008, A494, pp. 21–27.

[7] Schwartz, A. J., Kumar, M. and Adams, B. L. *Electron Backscatter Diffraction in Materials Science*, Kluwer Academic/Plenum Publishers, 2000.

[8] Bunge, H. J., "*Texture Analysis in Materials Science, Mathematical Methods*", Butterworths-Heinemann, Lodon, 1982.